OATAO
Open Archive Toulouse Archive Ouverte

Open Archive TOULOUSE Archive Ouverte (OATAO)

OATAO is an open access repository that collects the work of Toulouse researchers and makes it freely available over the web where possible.

Microstructure of $Ba_{1-x}La_xTiO_{3-\delta}$ ceramics sintered by Spark Plasma Sintering

N. El Horr [a,*], Z. Valdez-Nava [b,c], C. Tenailleau [a], S. Guillemet-Fritsch [a]

[a] *Institut Carnot CIRIMAT, Université Paul Sabatier, UMR CNRS 5085, 118 route de Narbonne, 31062 Toulouse Cedex 9, France*
[b] *Université de Toulouse, UPS, INPT, LAPLACE (Laboratoire Plasma et Conversion d'Energie), 118 route de Narbonne, F-31062 Toulouse Cedex 9, France*
[c] *CNRS, LAPLACE, F-31062 Toulouse, France*

Abstract

Nano-sized $Ba_{1-x}La_xTiO_3$ ($0.00 \leq x \leq 0.14$) powders were prepared by a coprecipitation method and calcined at 850 °C in air. The corresponding ceramics were obtained by Spark Plasma Sintering (SPS) at 1050 °C. These ceramics are oxygen deficient and are marked as $Ba_{1-x}La_xTiO_{3-\delta}$. Both powders and ceramics were characterized by X-ray diffraction (XRD) and Transmission Electron Microscopy (TEM). The effect of lanthanum concentration on the densification behavior, on the structure and the microstructure of the oxides was investigated. Average grain sizes are comprised between 54 (3) nm and 27 (2) nm for powders, and 330 (11) nm and 36 (1) nm for ceramics according to the La-doping level. Powders crystallize in the cubic (or pseudo-cubic) perovskite phase. The structure of ceramics consists in a mixture of cubic (or pseudo-cubic) and tetragonal perovskite type phases. As the lanthanum content increases, the tetragonality of the samples decreases, as well as the grain size.

Keywords: $BaTiO_3$; SPS; Microstructure; Grain size; Electron microscopy

1. Introduction

Since the 1940s, barium titanate $BaTiO_3$ (BTO), pure or doped with different elements has been the subject of many investigations, essentially because of its interesting properties (ferroelectric, dielectric, optical, pyroelectric, piezoelectric, etc.) which make it a very attractive material for the electronic industry[1–4] (thermistors, multilayer ceramic capacitors, pressure sensors, etc.). As miniaturization drives a branch of this industry, some barriers appear in conventional sintering processes, such as the grain size (GS), the sintering temperature and the purity. Therefore, new routes must be explored to produce this ceramic material.

It is well known that the GS of the material (powders and ceramics) represents one of the parameters which has a large effect on material properties, and has in consequence, a high impact on their specific applications. Several new powder synthesis methods and sintering processes have been reported in the literature in order to control the chemical and structural characteristics and thus the properties of the final product.

Recently, there has been a growing interest for Spark Plasma Sintering (SPS) technique. It offers, in comparison with the conventional sintering methods, the possibility of a very fast densification (generally several minutes only) which limits the grain growth. In other words, SPS is a rapid way for producing dense ceramics with small GS. This method has already been applied to obtain dense ceramics of BTO.[5–15] It has been shown that the use of SPS technique with fine BTO powders (from several nanometers to a few micrometers) prepared by various methods (hydrothermal, hydrolytic, sol–crystal methods, etc.), and also, the controlling of sintering conditions, allowed us to produce dense ceramics with GS ranging from 15 nm to several micrometers. Also, the SPS technique presents the advantage of using much lower sintering temperature, much shorter sintering time thus leading to inhibition of exaggerated grain growth when compared with conventional sintering methods. The properties of BTO can also be modulated by doping the material with rare-earth elements such as lanthanum (La).[16–19] If the behavior of La-doped BTO ceramics obtained using conventional sintering is well known,[20–28] understanding the effect of La-doping

* Corresponding author. Tel.: +33 5 62 25 82 53; fax: +33 5 62 25 82 77.
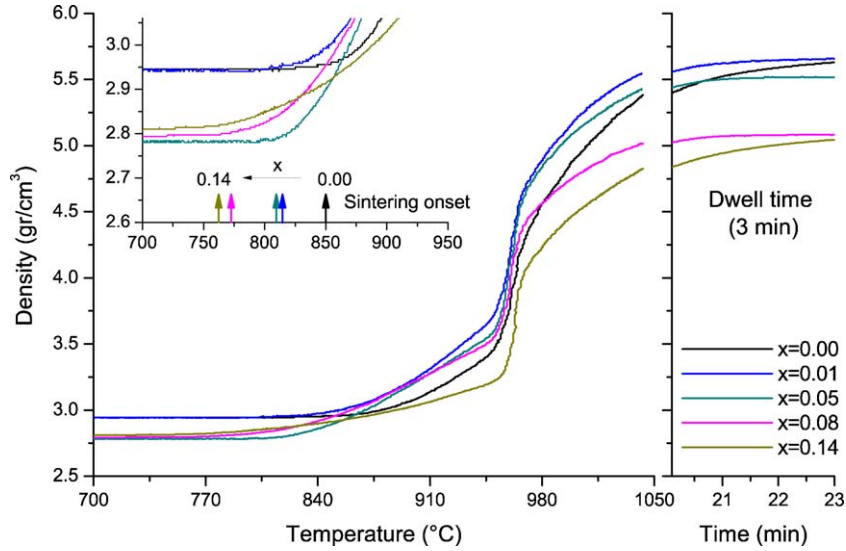*E-mail address:* nahida.el-horr@iut-tlse3.fr (N. El Horr).

Fig. 1. Densification curves of $Ba_{1-x}La_xTiO_3$ samples with $x = 0$, 0.01, 0.05, 0.08 and 0.14. The top-left inset shows an enlarged view of curves at the beginning of the densification. The curves shown in the right part of the figure correspond to time-dependent changes in density for each sample during the dwell time.

on SPS sintered BTO ceramics is still in progress.[29] This work presents a systematic study concerning the influence of La concentration on the GS, the structure and the densification behavior of $Ba_{1-x}La_xTiO_{3-\delta}$ ($x = 0, 0.01, 0.05, 0.08, 0.14$) oxides sintered by SPS.

2. Experimental procedure

2.1. Sample preparation

The La-doped BTO oxalate powders were first obtained using a coprecipitation reaction. The calcination treatment led to the oxide powders. The starting materials were $BaCl_2 \cdot 2H_2O$ (Prolabo), $TiCl_3$ (Prolabo, $d = 1.20$, % min = 15) and $LaCl_3 \cdot 7H_2O$

(Prolabo, 99%). They were dissolved in water in various proportions and the coprecipitation was performed by addition of a solution of oxalic acid dissolved in ethanol. $TiCl_3$ was chosen because it was easier to handle than $TiCl_4$. The full oxidation of Ti^{3+} in Ti^{4+} in the solution was ensured by air bubbling during the reaction which was evidenced by the color variation from brown to yellowish. The volume of water was taken much lower than the one of ethanol, in order to decrease the dielectric permittivity of the precipitation media. Since the nucleation of the particles is favored compared to their growth, smaller particles, homogeneous in size and composition, are likely to be obtained. The solution was aged for a couple of hours, and the obtained precipitate was centrifuged. The precursors were then pyrolized in air at 850 °C for 4 h to obtain the oxides.

Samples were sintered in a SPS apparatus (Sumitomo Coal Company – Dr Sinter 2080). The powders were placed in graphite die with a lining of graphite paper and heated under vacuum to a sintering temperature of 1050 °C with a holding
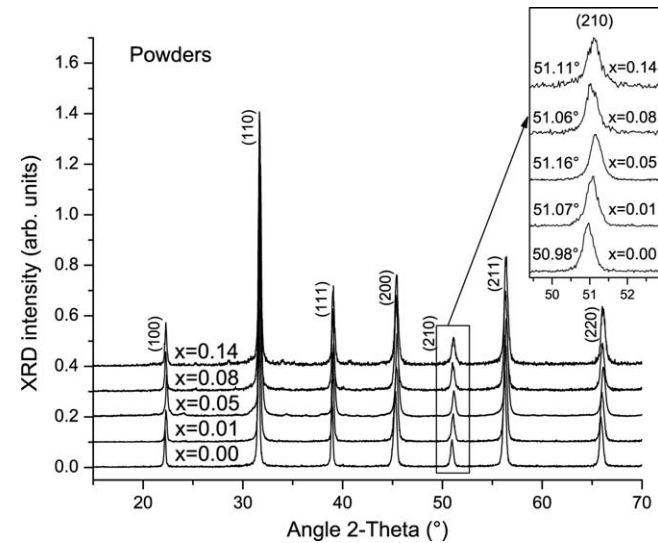

Fig. 2. XRD patterns of $Ba_{1-x}La_xTiO_3$ powders with $x = 0$, 0.01, 0.05, 0.08 and 0.14. The top-right inset represents an enlarged view of XRD patterns for $50° < 2\theta < 52°$ showing the (2 1 0) peak displacements with the variation of La content.

Table 1
Density and densification of $La_{1-x}Ba_xTiO_{3-\delta}$ ceramics.

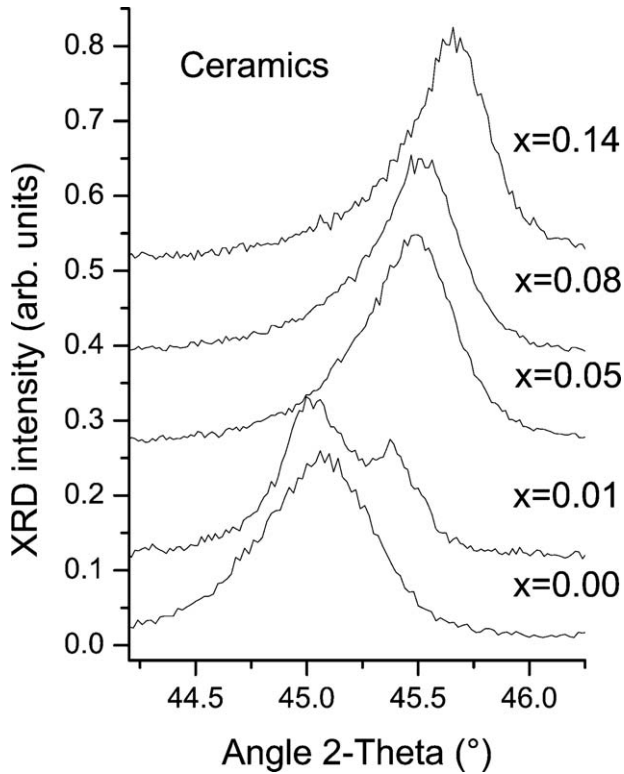|	La content (x)				
	0.00	0.01	0.05	0.08	0.14
Theoretical density of ceramics d_{th} (g/cm^3)	6.0	6.0	6.0	6.1	6.1
Green density d_1 (g/cm^3)	3.0	2.9	2.8	2.8	2.8
Density of ceramics after sintering d_2 (g/cm^3)	5.8	5.8	5.7	5.2	5.2
Densification (%)	96.7	96.7	95.0	85.2	85.2

Fig. 3. XRD patterns of $Ba_{1-x}La_xTiO_{3-\delta}$ ceramics with $x = 0$, 0.01, 0.05, 0.08 and 0.14, sintered at 1050 °C, for $44.25° < 2\theta < 46.25°$ showing the splitting of (0 0 2) and (2 0 0) peaks and showing the decrease of the tetragonality (i.e., the decrease of the magnitude of the peak splitting) with increasing La content.

time of 3 min. The shrinkage of the sample as a function of time was recorded during the overall process. A 50 MPa pressure was applied at 950 °C just after the sintering onset was observed. The pressure was maintained constant till the end of the dwell time at 1050 °C. After that, the pressure was removed, and the sample
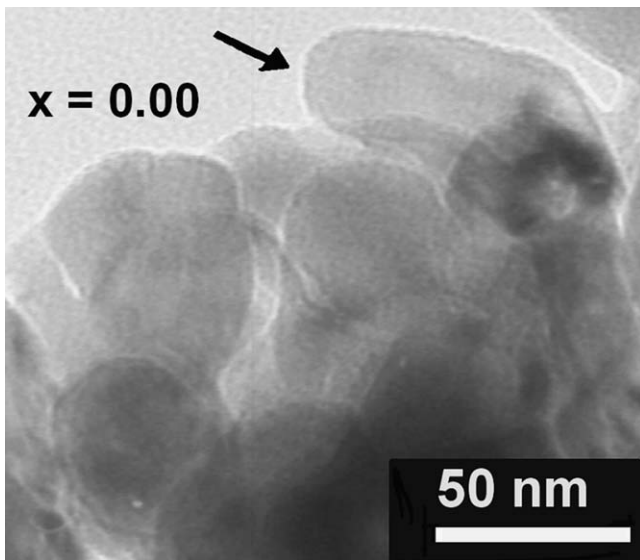

Fig. 4. Bright field TEM image of an undoped BTO powder sample showing grains which are in majority equiaxed ($D_{average}$ value = 54 nm). Elongated grain is marked by an arrow.
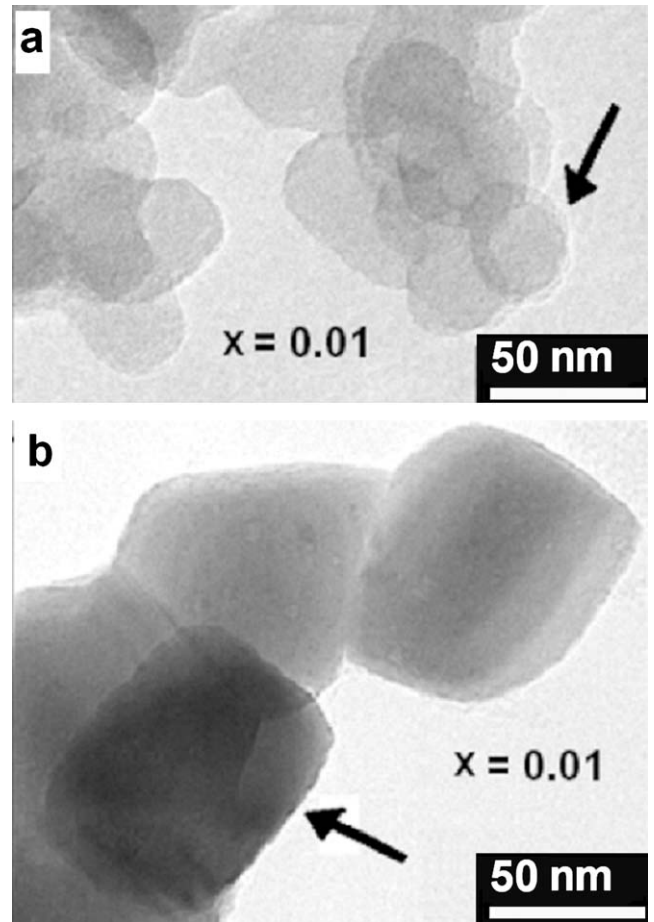

Fig. 5. Bright field TEM images of $Ba_{1-x}La_xTiO_3$ powder samples ($x = 0.01$) showing: (a) spherical shaped grains, as the grain marked by an arrow, and with GS value ∼27 nm; (b) tetragonal (close to quasi-cubic) and cubic shaped grains, as the grain marked by an arrow, and with GS much higher than those shown in (a).

was cooled to the room temperature by shutting down the power supply. The obtained samples were polished with SiC paper to remove carbon deposited on surface samples from the graphite paper during sintering.

2.2. Sample characterization

A Brucker D4 powder diffractometer was used to determine the X-ray diffraction (XRD) patterns for the oxide powders and the sintered ceramics. The diffractometer operated with an emitting source of Cu ($K\alpha_1, \alpha_2$ mean = 1.5418 Å).

The sample preparation of SPS sintered ceramics for Transmission Electron Microscopy (TEM) observations requires a lot of skills and deserves to be detailed. In fact the SPS samples are very brittle and have a mechanical behavior close to the one of glass.

A first block of sample was cut from the sintered pellets using a diamond saw (ESCIL 3032-4). This block was placed inside a brass tube (diameter = 3 mm) and bound with an epoxy resin (Gatan G1). Following epoxy polymerization (50 °C overnight) the tube was sliced into 500 micron thick discs using the same diamond saw. Mechanical polishing was done up to 100 microns
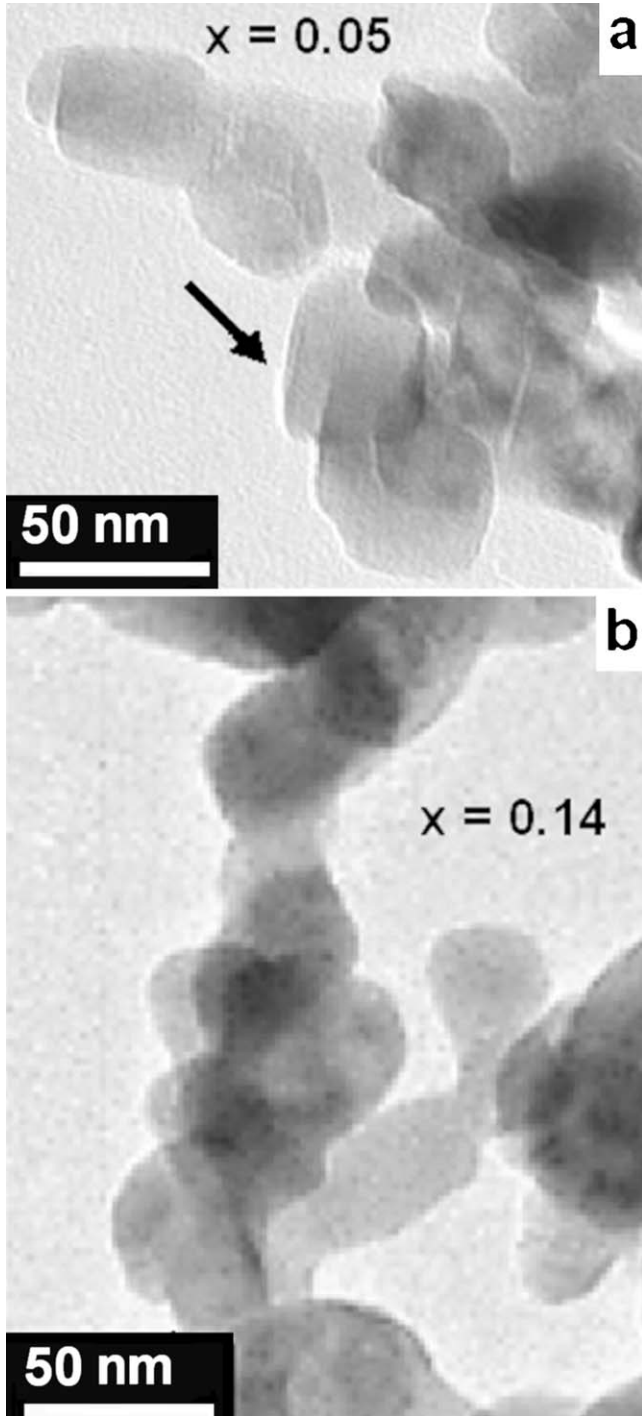
Fig. 6. Bright field TEM images of $Ba_{1-x}La_xTiO_3$ powder samples: (a) for $x = 0.05$ showing tetragonal (close to quasi-cubic) shaped grains for which one or more angles are round shape as the grain marked by an arrow; (b) for $x = 0.14$ showing that grains are equiaxed and their $D_{average}$ (about 28 nm) is lower than that of $x = 0.05$ (about 42 nm).

(ESCIL: ESC 300 GTL). At last, a concave dimple polishing (a EA-Fishione – model 2000 – polishing liquid: solution with diamond in suspension) followed by ion beam thinning (GATAN PIPS) were utilized to obtain a sample thickness of approximately 100 nm.

The samples (powders and ceramics) were observed using a JEOL JEM 2010 electron microscope operating at 200 kV. The electron beam was emitted from a LaB_6 single crystal cathode. The sample holder can be tilted around the x-axis or the y-axis and the amount of the tilt is $\pm30°$. The maximum resolution of this microscope is: 0.23 nm point point and 0.14 nm line line.

For each sample, the granulometric analyses of TEM images were realized using ImageJ software.[30]

3. Results

3.1. Densification

The green density and the densification after sintering of the various ceramics are reported in Table 1. The densification depends on the lanthanum content (x). For a given sintering temperature, i.e., 1050 °C, the highest value of relative density is 96.7% for pure BTO. The densification, then, decreases down to a value of 85.2% for $x = 0.08$ and $x = 0.14$.

The sintering curves are shown in Fig. 1 for each composition. The shrinkage onset temperature also depends on the La content (x): the highest value of x, the lowest the temperature of sintering onset. This temperature is 762 °C for $x = 0.14$ and increases to 812 °C for $x = 0.01$ and reaches 855 °C for $x = 0$. The kinetic of sintering, that is directly proportional to the slope of the curve, also strongly depends on the composition. In this case, a higher La content leads to a slower densification rate. So, both the onset temperature and the kinetic of sintering explain the decrease of density observed as the La content increases.

In previous work[29] we noticed that SPS sintering can cause an oxygen deficiency and minimal carbon pollution due to vacuum and the graphite matrix used to press and sinter the powders: CO_2 desorption experiments show that carbon contamination of the samples is minimal and final ceramics are oxygen deficient ($Ba_{1-x}La_xTiO_{3-\delta}$) when oxygen is dosed by EPMA (Electron Probe Microanalysis) and EELS (Electron Energy Loss Spectroscopy).

3.2. Structure

3.2.1. Powders

The X-ray diffraction (XRD) patterns of the nano-sized powders are reported in Fig. 2. The structure of each initial powder is a cubic (or pseudo-cubic) perovskite. This observation is consistent with the fact that BTO crystallizes in the cubic phase, when GSs are fine (belonging to the nanometric scale).[28,31–33] The patterns of $Ba_{1-x}La_xTiO_3$ fit with that of cubic BTO (JCPDS file 01-079-2263) pattern with slight shifts in peak positions towards higher angles. They indicate that the lattice parameter slightly decreases with an increase in La content. They are due to the difference in ionic radius between lanthanum and barium (La^{3+} ion size = 1.36 Å and Ba^{2+} ion size = 1.61 Å[34] in 12 coordinate for cubic phase).

The peaks are shifted on the right hand side for $0 \leq x \leq 0.05$ and for $0.08 \leq x \leq 0.14$. But the peaks are shifted towards lower values of 2θ for $0.05 \leq x \leq 0.08$; this unexpected behavior could be related to a particular phenomenon reported by different
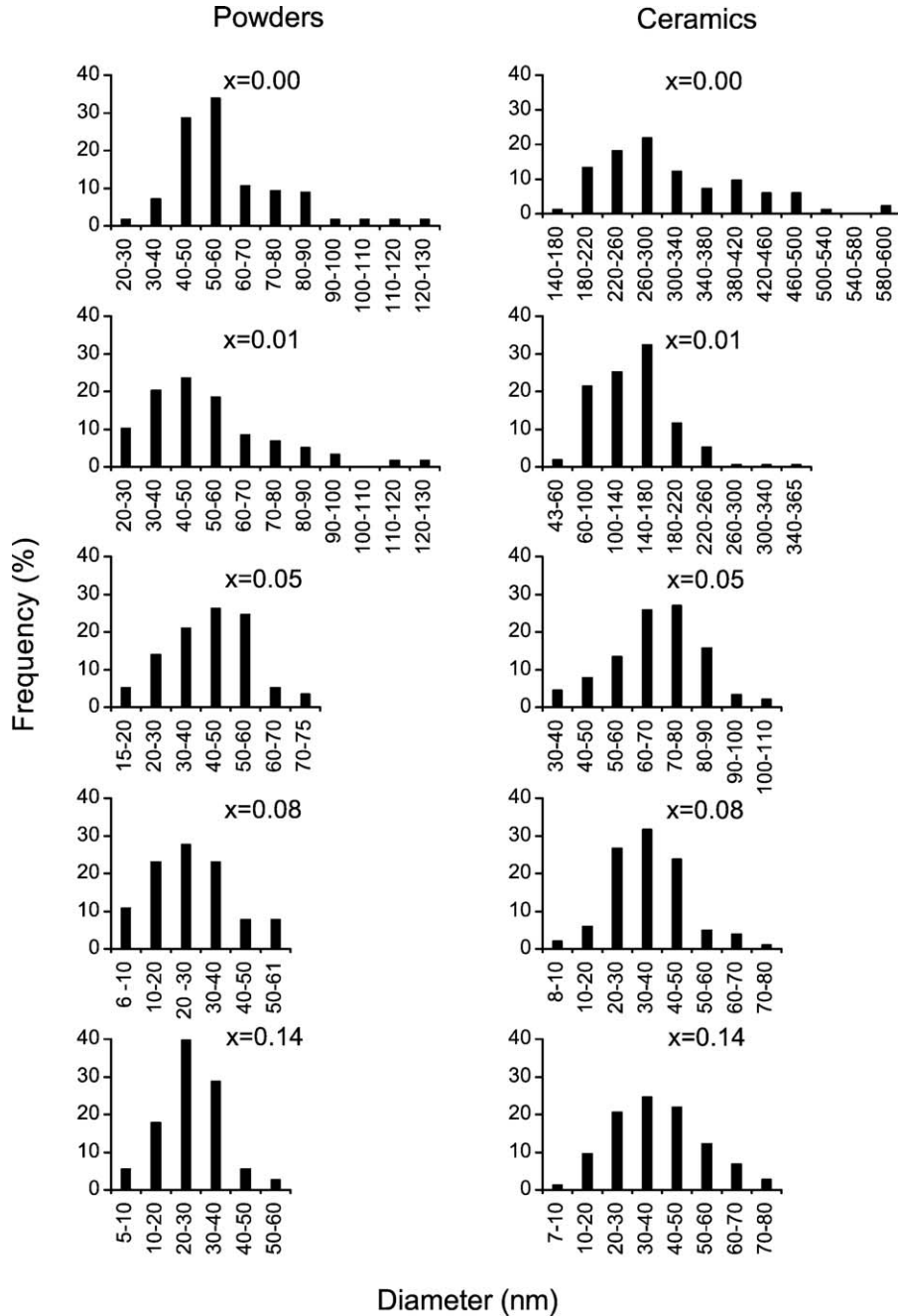
Fig. 7. Histograms of La-doped BTO samples (powders and ceramics obtained at 1050 °C) showing the change in sample GS distributions ($x = 0$, 0.01, 0.05, 0.08 and 0.14).

authors.[35–39] These authors showed that below a critical value of GS (~80 nm), the structure of BTO is cubic, and the lattice parameter increases as GS decreases and this phenomenon is amplified when GS is lower than 30 nm. So, in our case, the powder of composition $x = 0.05$ has a GS of 42 nm which is relatively high compared with that obtained for $x = 0.08$ (GS = 27 nm) and the associated increase in lattice parameter is large. Further doping, from $x = 0.08$ to $x = 0.14$, did not impact the average GS ($D_{average}$). So, the peak positions were influenced only by the increase of La-doping and were displaced in the expected direction, towards higher 2θ values.

3.2.2. Ceramics

For each ceramic sample, the part of XRD pattern that corresponds to $44.25° \leq 2\theta \leq 46.25°$, is shown in Fig. 3. For each composition, the splitting of the (2 0 0) peak ($2\theta = 45.234°$ in confirmity with JCPDS file 01-079-2263) into (0 0 2) and (2 0 0) peaks (with the respective values $2\theta = 45.092°$ and $45.510°$ – JCPDS file 01-074-1957) indicates the presence of the tetragonal phase. Moreover, the intensity ratio I_{002}/I_{200} of the two peaks is not equal to 0.5, and shows that the structure of the ceramics consists in a mixture of cubic (or pseudo-cubic) and tetragonal perovskite phases. The magnitude of the peak split-

ting, indicating the tetragonality, decreases as the lanthanum content increases. Since La^{3+} cations (ionic radius = 1.032 Å) substitute for larger Ba^{2+} cations (ionic radius = 1.35 Å)[34] on the A sites (in 6 coordinate for the tetragonal phase), there will be a decrease in the lattice value in the *c* direction, i.e., the *c/a* ratio tends towards 1.

3.3. Microstructure

3.3.1. Powders

TEM observations of the powder samples (Figs. 4–6) reveal that the grains are mostly equiaxed. Some spherical shaped grains are observed as shown by an arrow in Fig. 5a. This shape is observed among the small grains, i.e., for GS less than 27 nm and can be attributed to the cubic phase.[22,32] Some tetragonal (close to quasi-cubic) and cubic shaped grains (shown by an arrow in Fig. 5b) are also observed in some cases. One or more angles are sometimes rounded (shown by an arrow in Fig. 6a). Elongated grains (shown by an arrow in Fig. 4) are rarely observed. No defects or dislocations are noticed.

The GS distribution has been determined for each powder. The histogram of each sample is shown in Fig. 7. The characteristics of each distribution are reported in Table 2. An asymmetric monomodal dispersion has been observed for each sample, with a minima (D_{min}) of 5 nm ($x = 0.08$ and $x = 0.14$) and a maxima (D_{max}) of 140 nm (pure BTO sample). Only for the samples of composition $x = 0.08$ and $x = 0.14$, one can notice a distribution close to symmetric monomodal, i.e., normal distributions. For each GS distribution, the median GS (D_{median}) is equal or very close to the $D_{average}$ value. The spreads of overall GS distributions are slightly wide and no significant differences are noticed among them (like it is shown by the values of the relative standard deviation (RSD) of the dispersions (Table 2) which are approximately of the same order of magnitude).

The variation of $D_{average}$ value versus La concentration (for the powders) is represented in Fig. 8. The $D_{average}$ value is the same for pure BTO and for $x = 0.01$ (~54 nm), but the GS distribution of $x = 0.01$ sample is a little wider in comparison to the BTO one. The $D_{average}$ value decreased slightly (~42 nm) for $x = 0.05$ sample but then more significantly for $x = 0.08$ (~27 nm). A higher La content ($x = 0.14$) does not affect the $D_{average}$ value of the powders.

3.3.2. Ceramics

After sintering at 1050 °C, the ceramic grains remained mostly equiaxed (Figs. 9–11) quite similar to quadratic or cubic forms (with truncated or rounded angles). No particular defect is observed. The grains are monodomain and dislocation free.

The GS distribution has been determined for each ceramic. The histogram of each ceramic sample is shown in Fig. 7. The characteristics of each distribution are reported in Table 2. The variation of $D_{average}$ value versus La concentration, for these ceramic samples, is represented in Fig. 8. Although using SPS technique, and low sintering temperature (1050 °C), little grain growth occurs. The $D_{average}$ value of the dense ceramics is higher than the one of the initial powders and the D_{max} value determined
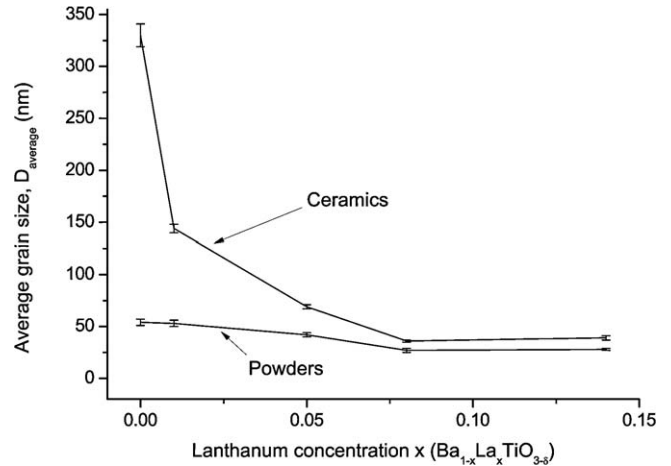

Fig. 8. $D_{average}$ value of $Ba_{1-x}La_xTiO_{3-\delta}$ powders and ceramics (obtained at 1050 °C) as a function of lanthanum concentration (x). Vertical bars represent σ, the uncertainty of $D_{average}$ ($\sigma^2 = \Sigma_{(i=1 \to N)} (D_i - D_{average})^2/N(N-1)$).

among all compositions is about 600 nm (for $x = 0$) as shown in Fig. 9.

The GS distributions of $x = 0.08$ and $x = 0.14$ samples are quite symmetrical. For the other ceramics, the distributions remain asymmetric. Moreover, the RSD values are smaller than the one of the powders, indicating better homogeneity for the majority of ceramics, except for the composition $x = 0.14$. The relative increase of the average size (RIAS) after sintering has been determined. It is the most important (RIAS = 511%) for pure BTO. It decreases to 172%, 64% and 33% for the respective compositions of ceramics: $x = 0.01$, 0.05 and 0.08. The presence of La in BTO seems to slow down the overall diffusion rate during the sintering process. The effect of La on grain growth and thus on the sintering mechanisms (with our sintering conditions), when x was varied from 0.08 to 0.14 can be described as follows: the $D_{average}$ value and the RIAS for $x = 0.08$ and $x = 0.14$ are approximately the same. For $x = 0.14$, the width of the histogram was wider than that for $x = 0.08$ and the percentage of small grains that were between 7 and 20 nm was higher for $x = 0.14$ than for $x = 0.08$. Although prior to sintering, the percentage of grains that ranged from 5 to 20 nm was higher for the powder containing

Fig. 9. Bright field TEM images of $Ba_{1-x}La_xTiO_{3-\delta}$ ceramic samples (obtained at 1050 °C) showing grains with sizes of 600 nm which correspond to the D_{max} value determined among all compositions.

Table 2
Grain size (D) of La$_{1-x}$Ba$_x$TiO$_{3-\delta}$ powders (Powd.) and ceramics (Ceram.) – the relative increase of average size (RIAS) is also reported.

	La content (x)				
	0.00	0.01	0.05	0.08	0.14
D_{min}–D_{max} (nm)					
Powd.	20–130	20–130	15–75	6–61	5–60
Ceram.	140–600	43–365	30–110	8–75	8–79
D_{median} (nm)					
Powd.	54	48	42	26	28
Ceram.	289	143	70	34	38
$D_{average}$ $(\sigma)^a$ (nm)					
Powd.	54 (3)	53 (3)	42 (2)	27 (2)	28 (1)
Ceram.	330 (11)	144 (4)	69 (2)	36 (1)	39 (2)
N^b					
Powd.	56	59	57	65	73
Ceram.	82	154	89	101	73
S^c (nm)					
Powd.	19	22	14	13	10
Ceram.	97	52	15	13	15
RSD^d					
Powd.	0.35	0.41	0.33	0.48	0.36
Ceram.	0.29	0.36	0.19	0.36	0.38
RIAS^e (%)	511	172	64	33	39

^{a} σ: uncertainty of the average size ($\sigma^2 = \Sigma_{(i=1 \rightarrow N)} (D_i - D_{average})^2/N(N-1)$).
^{b} N: number of measurements.
^{c} S: standard deviation of the dispersion ($S^2 = \Sigma_{(i=1 \rightarrow N)} (D_i - D_{average})^2/(N-1)$).
^{d} RSD: relative standard deviation of the dispersion (RSD $= S/D_{average}$).
^{e} RIAS: relative increase of average size $= [D_{average\,(ceram.)} - D_{average\,(powd.)}]/D_{average\,(powd.)}$.

0.08 La than for powder containing 0.14 La which could mean that the grain growth was slower for $x = 0.14$ than for $x = 0.08$. In addition to that, the densification curves (Fig. 1) showed that the densification rate is higher for the sample containing the smaller amount of La, i.e., $x = 0.08$ and the density of sample containing 0.08 La became stable after 1 min of dwell time but for the other sample (i.e., $x = 0.14$), the density continued to increase along the totality of the dwell time. So, the increase of La content from $x = 0.08$ to $x = 0.14$ had an effect both on the global GS and on the densification rate.

4. Discussion

The mechanisms occurring during the powder sintering are complex and depend on many factors (heating rate, applied pressure, particle size and distribution, etc.). All the processes that are involved during SPS sintering are not fully understood and some mechanisms are still under debate, such as plasma generation.[40–42] Among the mechanisms that are generally assumed during SPS sintering, we can mention: the surface, grain boundary

Fig. 10. Bright field TEM images of Ba$_{1-x}$La$_x$TiO$_{3-\delta}$ ceramic samples (sintered at 1050 °C): (a) for $x = 0$ showing grains which are equiaxed with a $D_{average}$ value of 330 nm; (b) and (c) for $x = 0.01$ showing equiaxed polydispersed grains which are smaller ($D_{average} = 144$ nm) than that for $x = 0.00$ and are quite similar to tetragonal or cubic forms (with truncated or rounded angles).
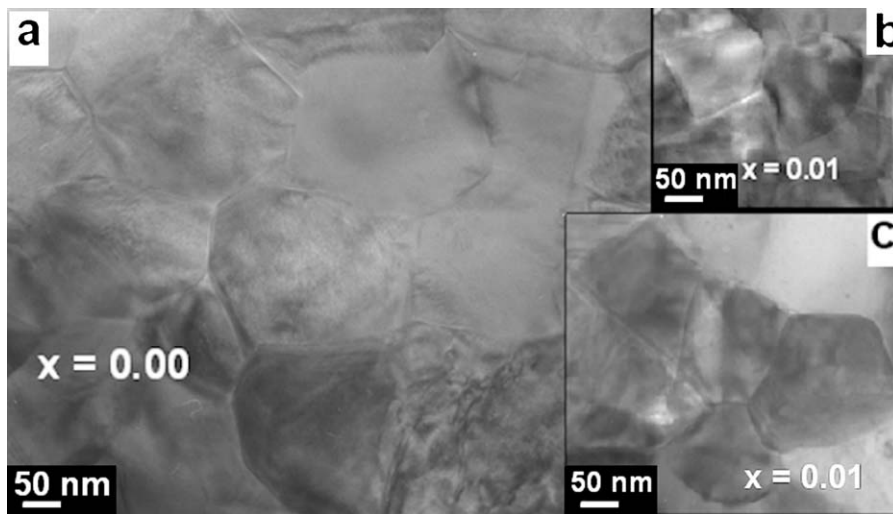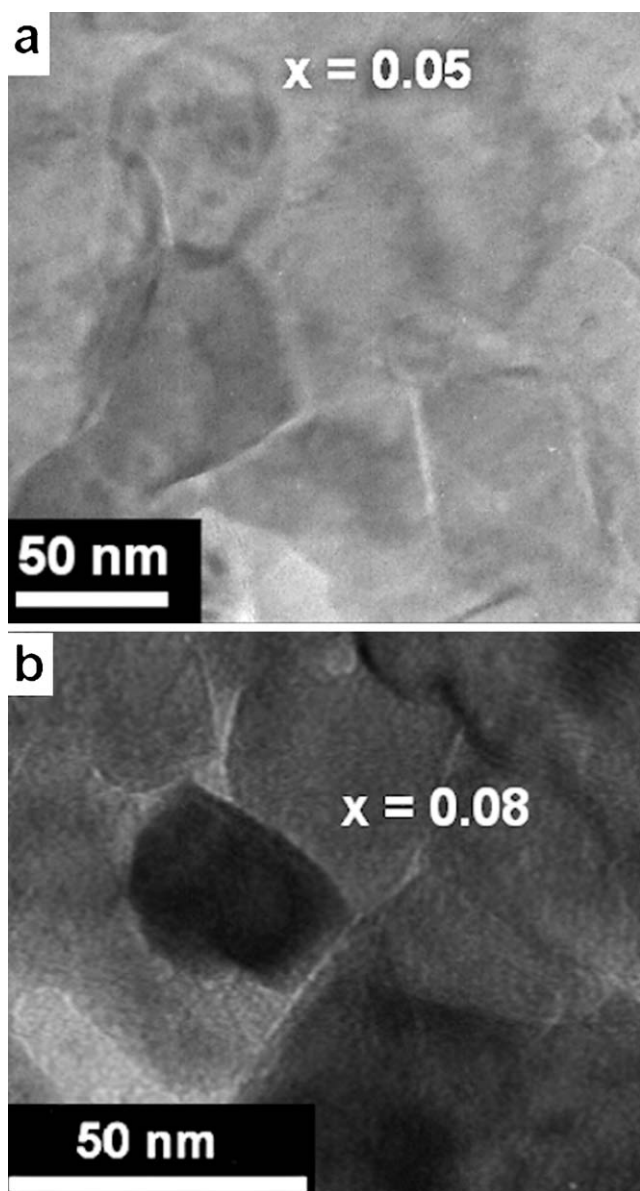
Fig. 11. Bright field TEM images of $Ba_{1-x}La_xTiO_{3-\delta}$ ceramic samples (sintered at 1050 °C): (a) for $x = 0.05$ showing grains which are equiaxed with a $D_{average}$ value of 69 nm; (b) for $x = 0.08$ showing equiaxed grains ($D_{average} = 36$ nm).

and volume diffusion; vaporization–condensation and plastic deformation.

In all our samples, the structures of initial powders are cubic (or pseudo-cubic) which is common for this type of nanograins BTO perovskites.[28,31–33] We have also observed an increase of the lattice parameter (displacing X-ray peak positions towards lower 2θ values) when x varies from 0.05 to 0.08, i.e., when the $D_{average}$ value was decreased from 42 nm to 27 nm as described by several authors.[35–39] The $D_{average}$ value of the starting powders lies between 54 and 27 nm. From Fig. 1, one can observe that the densification starts at lower temperature as the GS decreases. For example, the sintering onset appears at 762 °C for $x = 0.14$ ($D_{average} = 28$ nm) and 779 °C for $x = 0.08$ ($D_{average} = 27$ nm). This behavior could be related to the high surface energy and a surface diffusion in the early stages of sintering. At this stage,

particle growth is limited by the high heating rate, thus favoring the surface diffusion of species. As the GSs of green samples are small, the surface diffusion is preponderant and the densification starts early.[43] So, the sintering onset temperature increases systematically with the increase of the initial GS of samples, i.e., with the decrease of La content (805 °C for $x = 0.05$, 812 °C for $x = 0.01$) and reaches 855 °C for the sample showing the largest initial particle size, i.e., pure BTO ($D_{average} = 54$ nm). As the shrinkage begins and the temperature is further increased, the sintering is not only limited by surface diffusion anymore, but also limited by the bulk diffusion rate. Lanthanum doping obviously influences the densification rate, thus the sintering behavior. It is well known that BTO doped with a small amount of donor cations as lanthanum (>0.5 mol%), yields to cation vacancy compensation, i.e., oxygen vacancy and results in the material being fine-grained. When the lanthanum percentage increases, the number of oxygen vacancies becomes important and contributes to decrease the overall cationic transport, thus diminishing the diffusion rate and in consequence the densification rate.[44,45]

For the chosen sintering conditions, undoped BTO reached a maximum densification of 97% with a RIAS of grains of about 511%. For low La content ($x = 0.01$), with similar initial GS, the densification does not change, but the RIAS of grains is only 172%. This difference in the value of RIAS, clearly indicates that a small amount of La-doping has a big influence on the grain growth during the SPS sintering of $Ba_{1-x}La_xTiO_{3-\delta}$. This behavior could be the result of the formation of the oxygen vacancies by the introduction of La and also, the oxygen vacancies that are probably created during sintering, due to the reducing atmosphere inherent to the SPS process (vacuum in presence of the graphite die). The grain growth decreases as the La content increases (RIAS = 64% for $x = 0.05$ and 33% for $x = 0.08$).

The ceramics of compositions $x = 0.08$ and $x = 0.14$ show quite a different behavior, the densification is very low, only 85%. It is important to note that the RIASs of those ceramics are the lowest of the series, respectively 33% and 39%. As a consequence, the values of their $D_{average}$ are very low, 36 and 39 nm. This result is in agreement with previously reported results,[41,43] indicating that densification is enhanced by grain growth.

The variation of the $D_{average}$ value versus La concentration (for ceramics) is plotted in Fig. 8: for $0 < x < 0.08$ the $D_{average}$ value of ceramics was highly decreased (in this zone, the graph was similar to an exponential decay curve) and for $0.08 < x < 0.14$, the $D_{average}$ value of ceramics was approximately constant (about 36 nm). Then, these results showed that when the amount of La was increased from $x = 0$ to $x = 0.08$, the RIAS was decreased with the enhancement of La content, but, from $x = 0.08$ to $x = 0.14$, the increasing of La-doping did not show any significant effect on $D_{average}$ value. But, the observation of the overall results (histograms and densification curves) of $x = 0.08$ and $x = 0.14$ samples had shown that the grain growth in $x = 0.14$ sample occurred more slowly than that in $x = 0.08$ sample (the percentage of small grains ranged from 7 to 20 nm, observed in $x = 0.14$ sample was higher than those observed in $x = 0.08$ sample). In addition to that, the densification curves (Fig. 1) had

shown a decrease of densification rate when the composition was changed from $x = 0.08$ to $x = 0.14$.

Two hypotheses can be suggested in order to explain why the $D_{average}$ value of the ceramics did not change when x was increased from 0.08 to 0.14:

- The first hypothesis which is the more probable, is based on the fact that from a critical value of x (i.e., $x = 0.08$), the RIAS of grains (determined after sintering) reached its possible minimal value (with our sintering conditions) in a way that even if the La content was increased, the RIAS of grains cannot decrease any more. In other words, we can see that for $x = 0.08$, the initial GSs were already fine (between 6 and 61 nm with $D_{average} = 27$ nm) and their GSs were increased only very slightly after sintering (between 8 and 75 nm with $D_{average} = 36$ nm). So, there is an increase in the $D_{average}$ value of only 9 nm, which is very small. It is thus highly probable that if we increase the La content, the RIAS of grains after sintering will not change because it has reached a limit value.
- The second hypothesis is to consider that a change in La-doping mechanism may occur for a critical value of x (i.e., $x = 0.08$). It is probable that for $x < 0.08$, La^{3+} could occupy Ba-sites and for $x \geq 0.08$, La^{3+} could occupy both Ba-sites and Ti-sites.[46,47] However, this hypothesis is less probable than the previous one because lanthanum, among the rare earth elements, tends to occupy the Ba-sites.[26–28,47–49]

5. Conclusion

$Ba_{1-x}La_xTiO_{3-\delta}$ ceramics with $(0.00 \leq x \leq 0.14)$ and with $D_{average}$ value ranging from 330 (11) to 36 (1) nm were obtained using the SPS technique ($T_{sintering} = 1050\,^{\circ}C$, dwell time = 3 min) to nanometric powders (prepared by coprecipitation followed by a calcination at 850 °C) with $D_{average}$ values ranging from 54 (3) to 27 (2) nm. Both powders and ceramics were characterized by XRD and TEM. The initial powders correspond to the cubic (or pseudo-cubic) perovskite phase. An increase of the lattice parameter was observed when x varied from 0.05 to 0.08 (i.e., when the $D_{average}$ value was decreased from 42 nm to 27 nm). The structure of ceramics consists in a mixture of cubic (or pseudo-cubic) and tetragonal perovskite type phases (the tetragonality decreases with the enhancement of x). Lanthanum doping influences the densification rate, i.e., the sintering behavior. This behavior could be the result of the formation of the oxygen vacancies by the introduction of La. The highest is the value of x, the lowest are the temperature of sintering onset, densification rate, grain growth and thus density of ceramics. Doping in the $0 < x < 0.08$ range diminishes considerably the $D_{average}$ value of ceramics (from 330 nm to 36 nm) and for $0.08 < x < 0.14$, the $D_{average}$ value of ceramics remains approximately constant. Two hypotheses are proposed to explain why the $D_{average}$ value of ceramics did not change when x was increased from 0.08 to 0.14: either from a critical value of x (i.e., $x = 0.08$), the lowest limit value of the RIAS of grains could be attained (with our sintering conditions), either a change in La-doping mechanism might occur for $x \geq 0.08$ (for $x < 0.08$, La^{3+} could occupy Ba-sites and for $x \geq 0.08$, La^{3+} could occupy both

Ba-sites and Ti-sites). But the second hypothesis is less probable than the first one because that among the rare earth elements, lanthanum, in most cases, tends to occupy Ba-sites.

References

1. Kishi H, Mizuno Y, Chazono H. Base-metal electrode-multilayer ceramic capacitors: past, present and future perspectives. *Jpn J Appl Phys* 2003;**42**(Part 1, No. 1):1–15.
2. Haertling GH. Ferroelectric ceramics: history and technology. *J Am Ceram Soc* 1999;**82**(4):797–818.
3. Kutty TRN, Hari NS. Multifunctional cryogenic sensors from n-BaTiO$_3$ ceramics having strong negative temperature coefficient of resistance. *J Phys D: Appl Phys* 1995;**28**(2):371–4.
4. Lin PT, Yi F, Ho ST, Wessels BW. Two-dimensional ferroelectric photonic crystal waveguides: simulation, fabrication, and optical characterization. *J Lightwave Technol* 2009;**27**(19):4330–7.
5. Luan W, Gao L, Kawaoka H, Sekino T, Niihara K. Fabrication and characteristics of fine-grained BaTiO$_3$ ceramics by spark plasma sintering. *Ceram Int* 2004;**30**(3):405–10.
6. Takeuchi T, Bétourné E, Tabuchi M, Kageyama H, Kobayashi Y, Coats A, et al. Dielectric properties of spark-plasma-sintered BaTiO$_3$. *J Mater Sci* 1999;**34**:917–24.
7. Takeuchi T, Tabuchi M, Kageyama H, Suyama Y. Preparation of dense BaTiO$_3$ ceramics with submicrometer grains by spark plasma sintering. *J Am Ceram Soc* 1999;**82**(4):939–43.
8. Takeuchi T, Suyama Y, Sinclair DC, Kageyama H. Spark-plasma-sintering of fine BaTiO$_3$ powder prepared by a sol–crystal method. *J Mater Sci* 2001;**36**:2329–34.
9. Takeuchi T, Capiglia C, Balakrishnan N, Takeda Y, Kageyama H. Preparation of fine-grained BaTiO$_3$ ceramics by spark plasma sintering. *J Mater Res* 2002;**17**(3):575–81.
10. Wang X, Deng X, Li L. Processing, microstructure and properties of nanograin barium titanate ceramics by spark plasma sintering. *Mater Sci Forum* 2009;**606**(Advances in Ceramic Materials):135–47.
11. Zhao Z, Buscaglia V, Bowen P, Nygren M. Spark plasma sintering of nanocrystalline ceramics. *Key Eng Mater* 2004;**264–268**(Pt. 3, Euro Ceramics VIII):2297–300.
12. Buscaglia MT, Buscaglia V, Viviani M, Petzelt J, Savinov M, Mitoseriu L, et al. Ferroelectric properties of dense nanocrystalline BaTiO$_3$ ceramics. *Nanotechnology* 2004;**15**(9):1113–7.
13. Li B, Wang X, Li L, Zhou H, Liu X, Han X, et al. Dielectric properties of fine-grained BaTiO$_3$ prepared by spark-plasma sintering. *Mater Chem Phys* 2004;**83**(1):23–8.
14. Maiwa H. Preparation and properties of BaTiO$_3$ ceramics by spark plasma sintering. *Jpn J Appl Phys* 2008;**47**(9, Pt. 2):7646–9.
15. Li B, Wang X, Cai M, Hao L, Li L. Densification of uniformly small-grained BaTiO$_3$ using spark-plasma-sintering. *Mater Chem Phys* 2003;**82**(1):173–80.
16. Lu DY, Sun XY, Toda M. A novel high-k 'Y5V' barium titanate ceramics co-doped with lanthanum and cerium. *J Phys Chem Solids* 2007;**68**(4):650–64.
17. Morrison FD, Sinclair DC, West AR. Electrical and structural characteristics of lanthanum-doped barium titanate ceramics. *J Appl Phys* 1999;**86**(11):6355–66.
18. Morrison FD, Sinclair DC, Skakle JMS, West AR. Novel doping mechanism for very-high-permittivity barium titanate ceramics. *J Am Ceram Soc* 1998;**81**(7):1957–60.

19. Liu Y, Feng Y, Wu X, Han X. Microwave absorption properties of La doped barium titanate in X-band. *J Alloys Compd* 2009;**472**(1–2):441–5.

20. Jung DS, Koo HY, Jang HC, Kang YC. Effects of La content on the properties of $Ba_{1-x}La_xTiO_3$ powders prepared by spray pyrolysis. *Met Mater Int* 2009;**15**(5):809–14.

21. Jung DS, Lee SH, Kang YC. Effects of dopants on grain growth of nano-sized $BaTiO_3$ powders prepared by citric acid-assisted spray pyrolysis. *J Ceram Proc Res* 2008;**9**:307–10.

22. Xinle Z, Zhimei M, Zuojiang X, Guang C. Preparation and characterization on nano-sized barium titanate powder doped with lanthanum by sol–gel process. *J Rare Earths* 2006;**24**(Suppl. 1):82–5.

23. Morrison FD, Sinclair DC, West AR. Doping mechanisms and electrical properties of La-doped $BaTiO_3$ ceramics. *Int J Inorg Mater* 2001;**3**(8):1205–10.

24. Wenhu Y, Yongping PU, Xiaolong C, Jinfei W. Study of reoxidation in heavily La-doped barium titanate ceramics. *J Phys Conf Ser* 2009;**152**(1):012040.

25. Kuwabara M, Matsuda H, Kurata N, Matsuyama E. Shift of the Curie point of barium titanate ceramics with sintering temperature. *J Am Ceram Soc* 1997;**80**(10):2590–6.

26. Kishi H, Kohzu N, Mizuno Y, Iguchi Y, Sugino J, Ohsato H, et al. Effect of occupational sites of rare-earth elements on the microstructure in $BaTiO_3$. *Jpn J Appl Phys* 1999;**38**(9B):5452–6.

27. Xue LA, Chen Y, Brook RJ. The influence of ionic radii on the incorporation of trivalent dopants into barium titanate ($BaTiO_3$). *Mater Sci Eng B* 1988;**B1**(2):193–201.

28. Buscaglia MT, Buscaglia V, Viviani M, Nanni P, Hanuskova M. Influence of foreign ions on the crystal structure of $BaTiO_3$. *J Am Ceram Soc* 2000;**20**(12):1997–2007.

29. Valdez-Nava Z, Guillemet-Fritsch S, Tenailleau C, Lebey T, Durand B, Chane-Ching JY. Colossal dielectric permittivity of $BaTiO_3$-based nanocrystalline ceramics sintered by spark plasma sintering. *J Electroceram* 2009;**22**(1–3):238–44.

30. Abramoff MD, Magelhaes PJ, Ram SJ. Image processing with ImageJ. *Biophotonics Int* 2004;**11**(7):36–42.

31. Vijayalakshmi R, Rajendran V. Synthesis and characterization of cubic $BaTiO_3$ nanorods via facile hydrothermal method and their optical properties. *Dig J Nanomater Bios* 2010;**5**:511–7.

32. Zhu XH, Zhu JM, Zhou SH, Liu ZG, Ming NB, Hesse D. Microstructural characterization of $BaTiO_3$ ceramic nanoparticles synthesized by the hydrothermal technique. *Diffus Defect Data B* 2005;**106**(From Nanopowders to Functional Materials):41–6.

33. McHale JM, McIntyre PC, Sickafus KE, Coppa NV. Nanocrystalline $BaTiO_3$ from freeze-dried nitrate solutions. *J Mater Res* 1996;**11**(5):1199–209.

34. Shannon RD. Revised effective ionic radii and systematic studies of interatomic distances in halides and chalcogenides. *Acta Crystallogr A* 1976;**A32**(5):751–67.

35. Huang TC, Wang MT, Sheu HS, Hsieh WF. Size-dependent lattice dynamics of barium titanate nanoparticles. *J Phys Condens Matter* 2007;**19**(47):476212.

36. Valot C, Floquet N, Mesnier M, Niepce JC. Diffraction des rayons X par un polycristallin et microstructure en domaines ferroélectriques. *J Phys IV France* 1996;**06**(C4):71–89.

37. Perriat P. The Laplace law in finely divided powders. *Nanostructured Mater* 1995;**6**(5–8):791–4.

38. Caboche G, Niepce JC. Dielectric constant of fine grain $BaTiO_3$. In: Nair KM, Guha JP, Okamoto A, editors. *Ceramics transactions 32: dielectric ceramics: processing, properties and applications*. Westerville, OH: American Ceramic Society; 1993. p. 339–45.

39. Wada S, Yasuno H, Hoshina T, Nam SM, Kakemoto H, Tsurumi T. Preparation of nm-sized barium titanate fine particles and their powder dielectric properties. *Jpn J Appl Phys* 2003;**42**(9B):6188–95.

40. Chaim R. Densification mechanisms in spark plasma sintering of nanocrystalline ceramics. *Mater Sci Eng A* 2007;**443**(1–2):25–32.

41. Kim HT, Han YH. Sintering of nanocrystalline $BaTiO_3$. *Ceram Int* 2004;**30**(7):1719–23.

42. Aman Y, Garnier V, Djurado E. A screening design approach for the understanding of spark plasma sintering parameters: a case of translucent polycrystalline undoped alumina. *Int J Appl Ceram Tech* 2010;**7**(5):574–86.

43. Haussonne JM, Carry C, Bowen P, Barton J. Ceramics and glasses. In: *Principles and techniques of manufacture.* PPUR; 2005.

44. Shirasaki S, Yamamura H, Haneda H, Kakegawa K, Moori J. Defect structure and oxygen diffusion in undoped and La-doped polycrystalline barium titanate. *J Chem Phys* 1980;**73**(9):4640–5.

45. Shimanskij AF, Drofenik M, Kolar D. Subsolidus grain growth in donor doped barium titanate. *J Mater Sci* 1994;**29**(23):6301–5.

46. Reddy BS, Rao PK, Rao RMS. Effect of La substitution on the structural and dielectric properties of $BaZr_{0.1}Ti_{0.9}O_3$ ceramics. *J Alloys Compd* 2009;**481**(1–2):692–6.

47. Watanabe K, Ohsato H, Kishi H, Okino Y, Kohzu N, Iguchi Y, et al. Solubility of La–Mg and La–Al in $BaTiO_3$. *Solid State Ionics* 1998;**108**(1–4):129–35.

48. Itoh JI, Park DC, Ohashi N, Sakaguchi I, Yashima I, Haneda H, et al. Oxygen defects related to electrical properties of La-doped $BaTiO_3$. *Jpn J Appl Phys* 2002;**41**(6A):3798–803.

49. Tsur Y, Hitomi A, Scrymgeour I, Randall CA. Site occupancy of rare-earth cations in $BaTiO_3$. *Jpn J Appl Phys* 2001;**40**(1):255–8.